Virtual Internal Pair-Bond Model for Quasi-Brittle Materials

Kyoungsoo Park[1]; Glaucio H. Paulino[2]; and Jeffery R. Roesler[3]

Abstract: The present multiscale investigation employs the initial and total fracture energy through a virtual internal pair-bond (VIPB) model. The proposed VIPB model is an extension of the traditional virtual internal bond (VIB) model. Two different types of potentials, a steep short-range potential and a shallow long-range potential, are employed to describe the initial and the total fracture energies, respectively. The Morse potential function is modified for the virtual bond potential so that it is independent of specific length scales associated with the lattice geometry. This feature is incorporated in the VIPB model, which uses both fracture energies and cohesive strength. With respect to the discretization by finite elements, we address the element size dependence in conjunction with the *J* integral. Parameters in the VIPB model are evaluated by numerical simulations of a pure tension test in conjunction with measured fracture parameters. We also validate the VIPB model by predicting load versus crack mouth opening displacement curves for geometrically similar specimens, and the measured size effect. Finally, we provide an example involving fiber-reinforced concrete, which demonstrates the advantage of the VIPB model over the usual VIB model.

DOI: 10.1061/(ASCE)0733-9399(2008)134:10(856)

CE Database subject headings: Brittleness; Cracking; Models; Material properties.

Introduction

Interpreting structural behavior such as maximum load-bearing capacity is a relevant issue for structures containing quasi-brittle materials, especially concrete, because of their relatively large fracture process zone. The relatively large fracture process zone present in concrete results in the strength of a concrete beam in a laboratory-sized specimen being different from the strength of a concrete beam in an actual structure. This behavior is typically associated with the size effect (Bazant and Planas 1998; Bazant 1999, 2000). Therefore, in addition to experiments, appropriate physical assumptions and numerical techniques are necessary to predict and/or simulate fracture behavior of quasi-brittle materials.

One available numerical technique to simulate fracture behavior of materials is the cohesive zone model (CZM), which characterizes the nonlinear fracture process zone ahead of a crack tip. The concept was used by Barenblatt (1959) and Dugdale (1960). Hillerborg et al. (1976) expanded the concept to include concrete with linearly decreasing softening by combining fracture mechanics and the finite-element method. Hillerborg et al. (1976) utilized an equivalent nodal force, which corresponds to the linear traction–separation relationship. Later, based on the universal atomistic potential (Rose et al. 1981), Xu and Needleman (1994) introduced a cohesive surface element (the intrinsic CZM) for simulating generalized fracture within a finite element setting. This approach was extended to asphalt concrete by Paulino et al. (2004) and Song et al. (2006a,b), and to functionally graded material systems by Zhang and Paulino (2005). Recently, researchers have adaptively inserted the cohesive surface elements, e.g. the extrinsic CZM, to simulate crack propagation by using topological data structures (Pandolfi and Ortiz 2002; Zhang et al. 2007).

Another viable technique to characterize fracture behavior is the virtual internal bond (VIB) model, which integrates the macroscopic view of cohesive surfaces and the atomistic view of cohesive bonding between discrete particles (Gao and Klein 1998). Whereas the CZM separates fracture and elastic behaviors into a cohesive surface element and a bulk element, respectively, the VIB model represents both elastic and fracture behavior within the framework of continuum mechanics via the Cauchy–Born rule (Born 1940; Klein et al. 2001). Gao and Ji (2003) implemented the VIB modeling in nanomaterials demonstrating transition of the fracture mechanism from classical linear elastic fracture mechanics (LEFM) to homogeneous failure near the theoretical strength of solids. Moreover, Thiagarajan et al. (2004) have investigated dynamic fracture behavior for a brittle material under impact loading using the VIB model.

In order to characterize the relatively large fracture process zone in quasi-brittle materials, two different fracture energies, the initial fracture energy and the total fracture energy, are introduced by employing the concept of the equivalent elastic crack model (Bazant and Planas 1998; Shah et al. 1995). Roesler et al. (2007a) and Park (2005) have shown that both energies are essential to characterize concrete fracture behavior. *In order to consider two fracture energies, a virtual internal pair-bond (VIPB) model is proposed, which accounts for the relatively large fracture process zone and the size effect for quasi-brittle materials. Addi-*

[1]Graduate Research Assistant, Dept. of Civil and Environmental Engineering, Univ. of Illinois at Urbana-Champaign, 205 N. Mathews Ave., Urbana, IL 61801. E-mail: kpark16@uiuc.edu

[2]Donald Biggar Willett Professor of Engineering, Dept. of Civil and Environmental Engineering, Univ. of Illinois at Urbana-Champaign, 205 N. Mathews Ave., Urbana, IL 61801 (corresponding author). E-mail: paulino@uiuc.edu

[3]Associate Professor, Dept. of Civil and Environmental Engineering, Univ. of Illinois at Urbana-Champaign, 205 N. Mathews Ave., Urbana, IL 61801. E-mail: jroesler@uiuc.edu

Note. Associate Editor: Jiun-Shyan Chen. Discussion open until March 1, 2009. Separate discussions must be submitted for individual papers. The manuscript for this paper was submitted for review and possible publication on January 10, 2007; approved on February 21, 2008. This paper is part of the ***Journal of Engineering Mechanics***, Vol. 134, No. 10, October 1, 2008. ©ASCE, ISSN 0733-9399/2008/10-856–866/ $25.00.

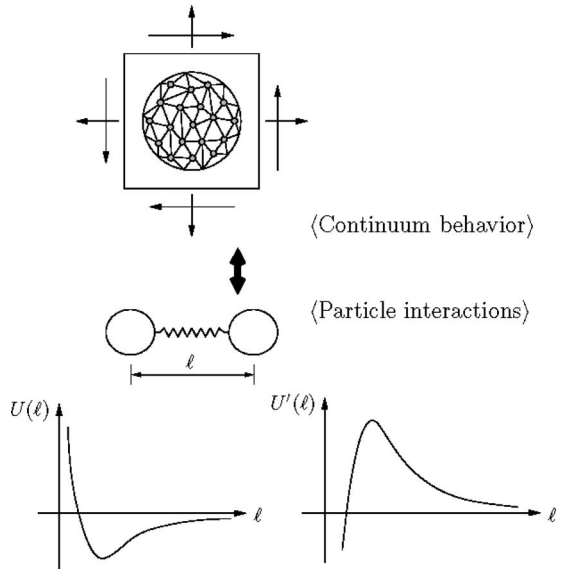

Fig. 1. Schematic illustration of the original VIB model

tionally, a modified Morse potential is utilized so that it is independent of any lattice parameter. The VIPB model thus characterizes essential macroscopic fracture parameters, i.e., fracture energies (initial and total) and cohesive strength of the material.

This paper is organized as follows. In the next section, the traditional VIB model formulation and a modified Morse potential function are presented for quasi-brittle materials. Then, the concept of the VIPB model is described in conjunction with two distinct fracture energies. The writers explain the determination of material properties including element size dependencies, and address verification and validation. Finally, the key findings of the present work are summarized.

Virtual Internal Bond Model Formulation

The VIB model (Gao and Klein 1998; Klein and Gao 1998) describes continuum behavior based on the microscopic interactions between particles within the concept of homogenization, as shown in Fig. 1. The microscopic behavior is connected to the macroscopic behavior by the Cauchy–Born rule, which results in the strain energy function (Tadmor et al. 1996). The VIB model represents both elastic and fracture behavior within the framework of continuum mechanics by using the macroscopic strain energy function. In the following, the VIB model formulation is reviewed, and a modified Morse bonding potential function, which represents the microscopic interactions between particles, is proposed.

Strain Energy Function in the VIB Model

The strain energy function in the VIB model is characterized by the bonding potential function via the Cauchy–Born rule. The Cauchy–Born rule is essentially a multiscaling assumption to connect atomistic behavior in the microlength scale with continuum behavior in the macrolength scale. Under this assumption, continuum behavior can be described by a single mapping function (i.e., deformation gradient $\mathbf{F}$)

$$\mathbf{F} = \frac{\partial \mathbf{x}}{\partial \mathbf{X}} \tag{1}$$

from the undeformed configuration (Lagrangian coordinates, $\mathbf{X}=X_I$) to the deformed configuration (Eulerian coordinates, $\mathbf{x}=x_i$). Therefore, the bonding potential $U(l)$ is defined by a deformed virtual bond length l along a bond direction $\boldsymbol{\xi}$

$$l = l_0\sqrt{\boldsymbol{\xi}\cdot\mathbf{F}^T\mathbf{F}\boldsymbol{\xi}} \tag{2}$$

where l_0=undeformed virtual bond length. Based on the bonding potential, the strain energy function (Φ) is represented by the summation of the bonding potential with a bond density $\mathcal{D}_\Omega$ over domain Ω

$$\Phi = \int U(l(\mathbf{F}))\mathcal{D}_\Omega d\Omega \tag{3}$$

If the bond direction $\boldsymbol{\xi}$ is specified by a three-dimensional spherical coordinate system, the strain energy function (3) is expressed by

$$\Phi = \langle U(l)\rangle \tag{4}$$

where

$$\langle\cdots\rangle = \int_0^{2\pi}\int_0^{\pi}\int_0^{l_0}\cdots\mathcal{D}_\Omega(\phi,\theta,l_0)\sin\theta\, dl_0 d\theta d\phi \tag{5}$$

and the bond direction vector is given as $\boldsymbol{\xi}=(\sin\theta\cos\phi,\sin\theta\sin\phi,\cos\theta)$.

For a two-dimensional plane stress problem, the strain energy function is expressed by

$$\Phi = \langle U(l)\rangle = \int_0^{2\pi}\int_0^{l_0} U(l)\mathcal{D}_\Omega(\phi,l_0)dl_0 d\phi \tag{6}$$

and the bond direction vector is selected by the circular coordinate system, $\boldsymbol{\xi}=(\cos\phi,\sin\phi)$.

In this study, a two-dimensional constant bond density function, $\mathcal{D}_\Omega=\mathcal{D}_0$, is considered, which illustrates an isotropic solid, and has the same initial bond length (l_0) over the domain. The constant bond density function simplifies the strain energy function to

$$\Phi = \langle U(l)\rangle = \mathcal{D}_0\int_0^{2\pi} U(l)d\phi \tag{7}$$

which is also suitable for numerical investigation of fracture properties.

Constitutive Relation

From the determination of the strain energy function (7), the constitutive relation is formulated on the basis of continuum mechanics. The Lagrangian strain $\mathbf{E}$ and the second Piola–Kirchhoff stress tensor $\mathbf{S}$ are used for computing the stress and the material modulus. The derivative of the strain energy with respect to the Lagrangian strain provides the second Piola–Kirchhoff stress

$$S_{IJ} = \frac{\partial\Phi}{\partial E_{IJ}} = \left\langle l_0^2\frac{U'(l)}{l}\xi_I\xi_J\right\rangle \tag{8}$$

Similarly, the material tangent modulus is obtained by the second derivative of the strain energy function with respect to the Lagrangian strain

J. Eng. Mech., 2008, 134(10): 856-866

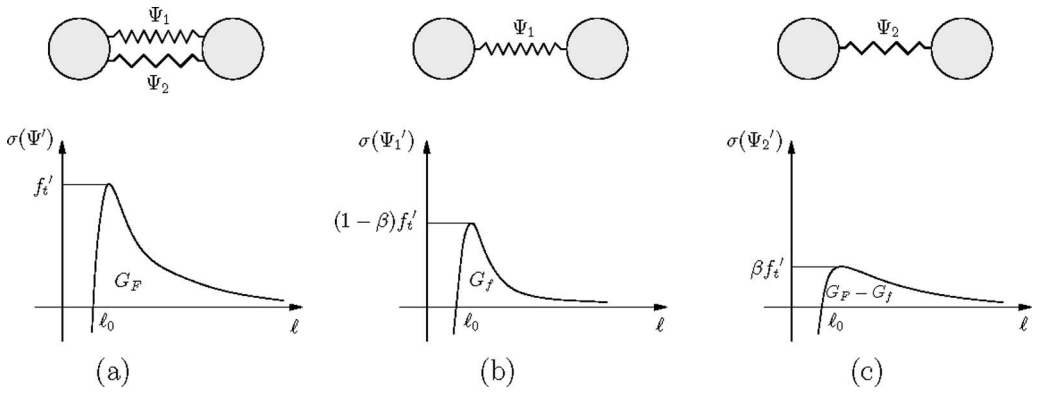

Fig. 2. Schematic illustration of the new VIPB model: (a) relationship between stress and bond length from the pair-bond potential ($\Psi=\Psi_1+\Psi_2$); (b) relationship from the steep short-range potential (Ψ_1); and (c) relationship from the shallow long-range potential (Ψ_2)

$$C_{IJKL}=\frac{\partial^2\Phi}{\partial E_{IJ}\partial E_{KL}}=\left\langle l_0^4\left(\frac{U''(l)}{l^2}-\frac{U'(l)}{l^3}\right)\xi_I\xi_J\xi_K\xi_L\right\rangle \tag{9}$$

which satisfies the Cauchy symmetry

$$C_{IJKL}=C_{IKJL} \tag{10}$$

in addition to the usual major and minor symmetries of elasticity. Because of these symmetries, only one elastic property is necessary. Therefore, the Cauchy symmetry is satisfied by the fourth-order isotropic elasticity tensor whose Lame parameters (μ,λ) are the same (Thiagarajan et al. 2004). Additionally, the VIB (or VIPB) model is hyperelastic and does not account for dissipation (unloading path is the same as the loading path).

Virtual Bond Density Potential

The focus of the VIB model is the determination of the virtual bond potential [$U(l)$] and the bond density function ($\mathcal{D}_0$), which describe both elastic behavior and fracture behavior. We define the bond density potential Ψ as the bond potential multiplied by a bond density function

$$\Psi(l)=\mathcal{D}_0U(l) \tag{11}$$

Previous researchers (Gao and Klein 1998; Klein and Gao 1998; Zhang et al. 2002; Klein et al. 2001; Nguyen et al. 2004; Thiagarajan et al. 2004) have employed a two-parameter (A,B) phenomenological cohesive law

$$\Psi'(l)=\mathcal{D}_0U'(l)=A(l-l_0)e^{-(l-l_0)/B} \tag{12}$$

for the bond density potential in the VIB model implementation. The constant A is related to the initial Young's modulus, whereas the constant B can be determined by the cohesive strength or by the fracture energy. Thus, this potential function can only characterize two material parameters: the initial elastic property and one fracture property.

In this study, the generalized Morse function (Morse 1929; Girifalco and Weizer 1959; Milstein 1973) is modified to represent the bond density potential and to characterize three macroscopic material parameters, specifically initial elastic modulus, fracture energy, and the cohesive strength. The modified Morse potential function is proposed herein as

$$\Psi(l)=\mathcal{D}_0U(l)=\frac{\mathcal{D}}{m-1}[e^{-m\alpha(l/l_0-1)}-me^{-\alpha(l/l_0-1)}] \tag{13}$$

The two exponents (m,α) in the potential function can characterize two fracture parameters: the cohesive strength and the fracture energy. The parameter $\mathcal{D}$ is associated with one elastic property, i.e., Young's modulus. Further, the potential function is independent of the lattice parameter (l_0) because the particle distance (l) is normalized with respect to the lattice parameter (l_0), which is not the case in the original Morse potential.

Computational Implementation

Numerical simulations of the VIB (or VIPB) model can be implemented by using a commercial software, e.g. ABAQUS, with the application of the user material (UMAT) subroutine. If the software uses the Cauchy stress ($\boldsymbol{\sigma}$) rather than the second Piola–Kirchhoff stress ($\mathbf{S}$) for the stress update scheme, then we must transform the second Piola–Kirchhoff stress into the Cauchy stress with the known relationship [see, for example, Belytschko et al. (2000)]

$$\boldsymbol{\sigma}=\frac{1}{\det(\mathbf{F})}\mathbf{F}\mathbf{S}\mathbf{F}^T \tag{14}$$

Virtual Internal Pair-Bond Model

The fracture energy and the cohesive strength are basic quantities to describe material fracture behavior. For quasi-brittle materials, especially concrete, two different energies are necessary for explaining the size effect (Bazant and Becq-Giraudon 2002). The initial fracture energy (G_f) is size independent and is based primarily on the peak load. The other quantity is the total fracture energy (G_F), which is specimen size dependent. The proposed VIPB model considers both fracture energies in order to capture the measured size effect.

In the VIPB model, two bonding density potentials are connected between two particles, as shown in Fig. 2(a). One steep short-range potential, $\Psi_1(l)$, Fig. 2(b), is related to the initial fracture energy, and a longer-range shallower potential, $\Psi_2(l)$, Fig. 2(c), is associated with the difference between the initial fracture energy and the total fracture energy. The summation of

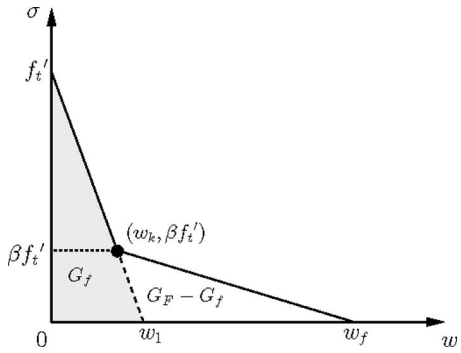

Fig. 3. Bilinear softening model for concrete where f_t'=tensile strength; G_f=initial fracture energy; G_F=total fracture energy; β=strength ratio at the kink point; w_1=horizontal axis intercept of the initial descending line; w_k=crack opening width at the kink point; and w_f=final crack opening width—see Park (2008)

each potential represents the bond density potential function of the VIPB model as illustrated in Fig. 2(a)

$$\Psi(l) = \Psi_1(l) + \Psi_2(l) \tag{15}$$

where

$$\Psi_i(l) = \frac{\mathcal{D}_i}{m_i - 1}[e^{-m_i\alpha_i(l/l_0-1)} - m_i e^{-\alpha_i(l/l_0-1)}] \quad (i = 1,2) \tag{16}$$

In this model, one bond density potential (Ψ_1), represented by G_f, is independent of the size so that the VIPB model characterizes the size effect. Another bond density potential (Ψ_2), described by ($G_F - G_f$), depends on the specimen size to satisfy the size dependence of the total fracture energy.

Each potential function contains three unknown constants ($\mathcal{D}_i$, m_i, and α_i) which can be determined by an elastic property (elastic modulus), and fracture properties (fracture energy and cohesive strength). The elastic and fracture properties are defined in each of the respective bond density potential function (Ψ_1 and Ψ_2). The fracture energy is separated into G_f and ($G_F - G_f$), as previously discussed.

The cohesive strength of the steep short-range potential is assumed then to be $(1-\beta)f_t'$, whereas that of the longer-range shallower potential is assumed to be $\beta f_t'$, as shown in Figs. 2(b and c). The strength ratio (β) of the two potentials can be defined as the kink point stress ratio in the bilinear softening model described in Fig. 3 (Park 2008). Because the kink point in the bilinear softening model is related to a postpeak load behavior, the long-range potential characterizes a postpeak load behavior in the VIPB model. The initial elastic modulus of each potential is determined under the assumption of linear elasticity at small strain. The elastic modulus of the pair-bond potential model is the summation of each potential, $E = E_1 + E_2$, because the bonds are connected in parallel. Each elastic modulus can, therefore, be defined by the same ratio as the cohesive strength for each potential.

The concept of the VIPB model is extended to characterize material responses of fiber-reinforced concrete (FRC). Fracture mechanisms of FRC generally consist of aggregate bridging and fiber bridging zones (Anderson 1995; Van Mier 1996). The aggregate bridging zone describes the crack branching and interlocking which result from the weak interface between the aggregates and cement matrix. The fiber bridging zone represents the effect of fibers on the stress transfer at larger opening displacements. The aggregate bridging zone is illustrated by the steep short-range potential, whereas the fiber bridging zone is described by the shallow long-range potential. The steep short-range potential (Ψ_1) is associated with the total fracture energy of plain concrete, and the shallow long-range potential (Ψ_2) is related to the difference between the total fracture energy of plain concrete (G_F) and the total fracture energy of FRC (G_{FRC}).

Determination of Material Properties

As the proposed VIPB model is based on the same framework of continuum mechanics as the VIB model, elastic and fracture properties are investigated in conjunction with the traditional VIB model. In the VIB model, elastic properties are examined at the state of infinitesimal strain and fracture properties are evaluated with respect to element size dependencies (Klein and Gao 1998). Therefore, previous studies provide the basis for the material properties to be used in both the VIB model and the VIPB model.

Elastic Properties at Infinitesimal Strains

Elastic material properties of the VIB (or VIPB) model can be evaluated at the state of small strain by defining the material tangent modulus in two different ways (Gao and Klein 1998). Either the strain energy function of the VIB (or VIPB) model or the linear elastic strain energy function represents the material tangent modulus. For the calculation of the material tangent modulus, the linearized strain is utilized because strain at the elastic range is infinitesimal.

First, the material tangent modulus is calculated by the strain energy function (4) of the VIB (or VIPB) model. Assuming infinitesimal strain, and taking a Taylor series expansion of the strain energy function and its second derivative with respect to the linearized strain, one obtains the material tangent modulus

$$C_{ijkl} = \frac{4\pi}{15} l_0^2 \Psi''(l_0)(\delta_{ij}\delta_{kl} + \delta_{ik}\delta_{jl} + \delta_{il}\delta_{kj}) \tag{17}$$

described by a bond density potential function, $\Psi(l)$, of the VIB (or VIPB) model.

Alternatively, the elastic modulus can also be obtained by the theory of linear elasticity. As the strain is assumed to be linear, the strain energy function is quadratic. Taking the second derivative with respect to the linearized strain, one obtains the material tangent modulus, as expected

$$C_{ijkl} = \lambda\delta_{ij}\delta_{kl} + \mu(\delta_{ik}\delta_{jl} + \delta_{il}\delta_{kj}) \tag{18}$$

From the Cauchy symmetry relation (10), the two Lame parameters are assumed to be the same ($\lambda = \mu$) in the material tangent modulus. As a result, equating Eqs. (17) and (18) results in the relationship between the shear modulus and the bond density potential function

$$\mu = \frac{4\pi}{15} l_0^2 \Psi''(l_0) \tag{19}$$

for a three-dimensional problem. The elastic properties are also represented by the Poisson's ratio (ν) and Young's modulus (E) whose relationships are

J. Eng. Mech., 2008, 134(10): 856-866

$$\nu = \frac{1}{4}, \quad E = \frac{2\pi}{3} l_0^2 \Psi''(l_0) \tag{20}$$

Moreover, for two-dimensional plane stress problems, the relationship between the shear modulus and the bond density potential energy function is

$$\mu = \frac{\pi}{4} l_0^2 \Psi''(l_0) \tag{21}$$

and Hooke's law leads to

$$\nu = \frac{1}{3}, \quad E = \frac{2\pi}{3} l_0^2 \Psi''(l_0) \tag{22}$$

The initial Young's modulus has been formed to correlate with the bond density potential (11), under the Cauchy symmetry condition ($\lambda = \mu$). Therefore, a constant $\mathcal{D}_i$ ($i=1,2$), in the bond density potential is determined from the relationship between the Young's modulus and the bond density potential function [Eqs. (20) and (22)] of the VIPB model. Substitution of Eq. (16) into Eq. (22) leads to

$$\mathcal{D}_i = \frac{3E_i}{2\pi m_i \alpha_i^2} \quad (i = 1,2) \tag{23}$$

which provides the closed form of the bond density function in terms of the elastic modulus and the two exponents (m_i, α_i) in the bond density potential. The exponents (m_i, α_i) can be associated with two fracture properties of materials, i.e., the fracture energy and the cohesive strength.

Fracture Properties and Mesh Size Dependencies

The essential fracture parameters for Mode I fracture are cohesive strength and fracture energy. These experimental fracture properties are utilized to estimate the two exponents (m_i, α_i) in the bond density potential through numerical simulations, e.g., the pure tension test (as discussed in the next section). In the simulation of a pure tension example, the numerical cohesive strength is assumed to be the peak stress in the pure tension test, whereas the numerical fracture energy is obtained from the area under the stress-displacement curve in the simulation. The two exponents (m_i, α_i) in the bond potential can then be determined by curve fitting; the two numerical fracture parameters (strength and fracture energy) obtained by a pure tension simulation coincide with known material properties from experiments.

In the VIB (or VIPB) model, the fracture energy depends on the element size (Klein et al. 2001), which can be explained by the path independent J integral (Rice 1968)

$$J = \int_\Gamma (U_0 \delta_{IJ} - P_{iJ} F_{iI}) N_J d\Gamma \tag{24}$$

where Γ=contour in the undeformed configuration surrounding the crack tip; U_0=strain energy density; $\mathbf{P}$=First Piola–Kirchhoff stress; and $\mathbf{N}$=outward normal to the contour, as shown in Fig. 4(a). Because of path independence, a contour is selected along the upper and lower bound (Γ^+ and Γ^-) of the localization zone (h_L) where stress softening occurs [Fig. 4(b)] for a Mode I loading (Klein and Gao 1998). The contour results in the symmetric stress and displacement field, and then we obtain J for Mode I

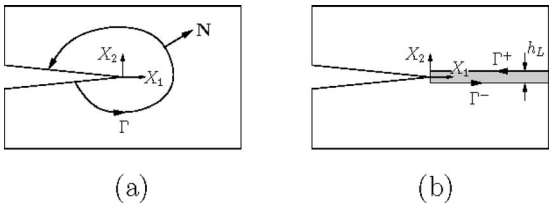

Fig. 4. J-integral contours (a) for an arbitrary path; (b) for a path of the localization zone

$$J = h_L \int_1^\infty P_{22} d\lambda_2 = G_I \tag{25}$$

where λ_2=stretch along the X_2 direction. Therefore, the J integral introduces a length scale (h_L) which is proportional to the fracture energy in the VIB (or VIPB) model. Because of this relationship, one should consider a length scale (e.g., localization zone size) for the simulation of the VIB (or VIPB) model. Further, the relationship provides guidance for verification studies and for determination of fracture parameters, discussed in the next section.

In summary, cohesive strength and fracture energy are considered in conjunction with the localization zone size to determine the exponents (α_i, m_i) in the bond density potential. First, one selects the localization zone size. Next, the exponents are calibrated by numerical simulation, e.g., the pure tension test, which provides two numerical fracture parameters (cohesive strength and fracture energy) which are consistent with expected values of experiments.

Verification: Fracture Properties and Element-Size Dependence

The fracture behavior of the VIB (or VIPB) model is analyzed by performing both the pure tension and the double cantilever beam (DCB) tests. Because numerical simulations of the pure tension example are associated with the measured cohesive strength and the fracture energy, the simulations enable us to determine the two exponents (m_i and α_i) with respect to the localization zone size (h_L). Additionally, the DCB test verifies the relationship between the fracture energy and the size of the localization zone, h_L, derived from the J integral. Moreover, in order to illustrate that the localization zone size is proportional to the fracture energy obtained by the numerical simulations of the DCB example, each numerical test has two different finite element mesh sizes for the localization zone where the VIB (or VIPB) element is defined. The main difference between the pure tension and the DCB examples is that the localization zone is taken as the entire domain in the former example, whereas it is taken as a (single element) strip in the latter example.

The determination of the bond density potential for the VIB model correlates with three measured concrete material properties: the Young's modulus (E=32 GPa), the cohesive strength (f_t'=4.15 MPa), and the reference fracture energy (G_{F0}=164 N/m). The bond density potentials for the VIPB model are associated with additional measured fracture parameters, i.e., initial fracture energy (G_f=56.6 N/m), and the strength ratio (β=0.34).

As the fracture energy (G_F) depends on the localization zone size (h_L) related to the VIB (or VIPB) element size, the reference fracture energy (G_{F0}) is defined at a reference localization zone

J. Eng. Mech., 2008, 134(10): 856-866

Table 1. Relationship between the VIB Element Size and the Fracture Energy

Computational test specimen	VIB element size (h_L) (m)	Total fracture energy: G_F-h_L relation (26) (N/m)	Total fracture energy: Numerical simulation result (N/m)
Pure tension	1	328,000	328,302
	0.5	164,000	164,311
DCB	h_{L0}=0.0005	G_{F0}=164	164
	0.00025	82	82

size (h_{L0}=0.5 mm). As shown in Table 1, if the size of the localization zone (h_L) grows in the finite element mesh, the numerical result of the fracture energy (G_F) also increases with the same ratio as that of the localization zone

$$G_F = G_{F0}\frac{h_L}{h_{L0}} \tag{26}$$

This relationship follows from expression (25), derived for the J integral.

Pure Tension Test

The pure tension numerical simulation has a square (W by W) domain, elongated at the top under displacement control. The numerical results for two different plate sizes (W=1 and 0.5 m) are provided in Fig. 5. The peak stress of the plate corresponds to the cohesive strength of 4.15 MPa. For the evaluation of the macroscopic numerical fracture energy, we calculate the area under the stress-displacement curve up to 40% elongation (chosen arbitrarily) of the virtual bond length (l) with respect to the undeformed virtual bond length (l_0). The calculated numerical fracture energy almost coincides with the analytical expression in Eq. (26), as shown in Table 1. Numerically, the area under the curve of the 1 m by 1 m plate is nearly twice that of the 0.5 m by 0.5 m plate. The bigger plate has twice the localization length of the smaller one. These numerical results illustrate that the fracture energy is proportional to the localization zone size in the VIB (or VIPB) model.

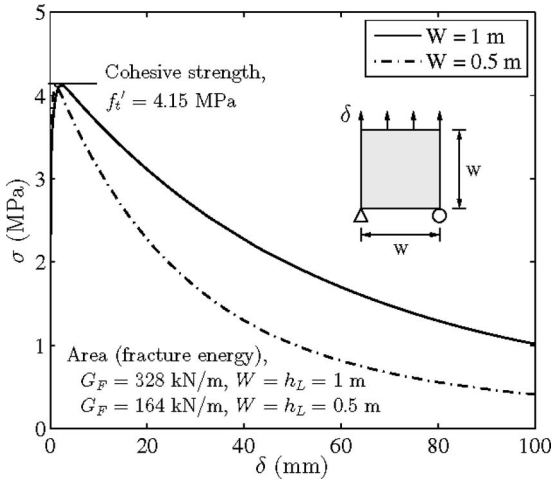

Fig. 5. Numerical simulation result of a pure tension test using the VIB model with different domain sizes (W=1 and 0.5 m). The loading is performed with displacement control (δ).

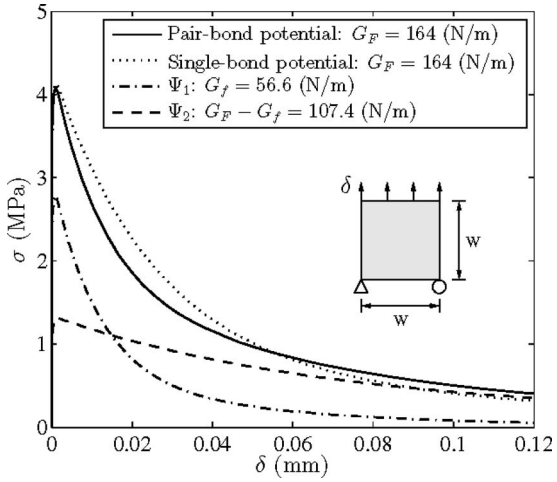

Fig. 6. Comparison between the VIB (single-bond) model and the VIPB (pair-bond) model with the localization zone size of $W=h_L$=0.5 mm. The loading is performed with displacement control (δ).

In addition, the VIPB (pair-bond potential) model is compared to the VIB (single-bond potential) model in Fig. 6, displaying results of the pure tension test with a localization zone size of 0.5 mm. The VIPB model results are indicated by a solid line for the stress-displacement curve, whereas the VIB model results are given by a dotted line. Each potential (Ψ_1,Ψ_2) for the VIPB model is represented by dashed lines. Both the VIB and the VIPB model have the same fracture energy and cohesive strength, but exhibit different postpeak load behavior. The different postpeak load behavior influences the maximum load capacity of structures containing quasi-brittle materials.

Double Cantilever Beam Test

The geometry of the DCB test is described in Fig. 7(a). It has initial notch (a_0) of 0.1 m, height ($2h$) of 0.1 m, and length (L) of 1 m. The DCB mesh detail around the crack tip [boxed area in Fig. 7(a)] is shown in Fig. 7(b), and the localization zone is defined by the VIB (or VIPB) element along the direction of crack propagation. Material properties are also the same as in the pure tension test in order to relate the fracture energy to the localization zone size. Elements outside the localization zone are defined as linear elastic.

The numerical simulation of the DCB is implemented with two different VIB (or VIPB) element sizes (h_L=0.5, 0.25 mm), with the same original geometry and with the same constants in the bond density potential function. Fig. 7(c) demonstrates the vertical stress (σ_{yy}) distribution under the deformed shape. The maximum stress corresponds to the cohesive strength (4.15 MPa), and the fracture behavior is localized with the large deformation where the VIB (or VIPB) element is defined.

Fig. 8 illustrates the agreement of the numerical results and the analytical solution of LEFM. For the size of 0.5 mm, the numerical results of the VIB model and the VIPB model are plotted in Fig. 8(a) with the LEFM analytical solution whose fracture energy is 164 N/m. Similarly, the localization zone size is 0.25 mm for the numerical simulation [Fig. 8(b)], and the fracture energy is 82 N/m for the analytical solution of LEFM. Additionally, the

J. Eng. Mech., 2008, 134(10): 856-866

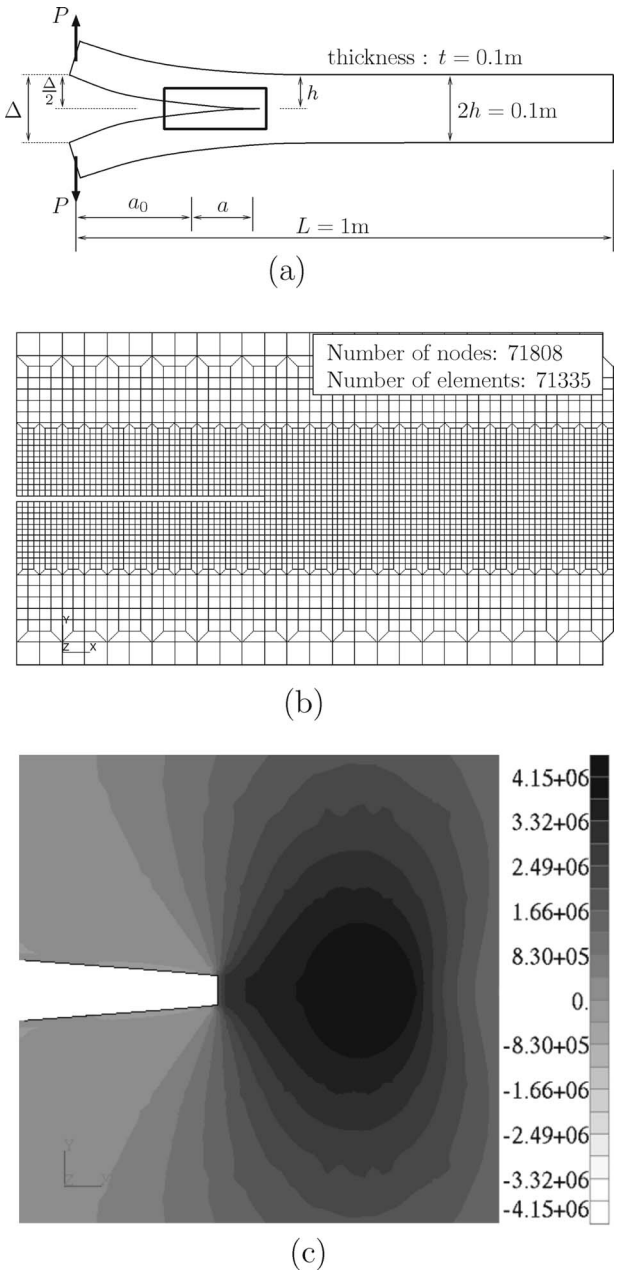

Fig. 7. (a) The geometry of the DCB test; (b) mesh detail around initial notch with the element size varying from 0.5 mm (localization zone) to 2 mm (outer region); and (c) normal stress, σ_{yy}, distribution under the deformed shape

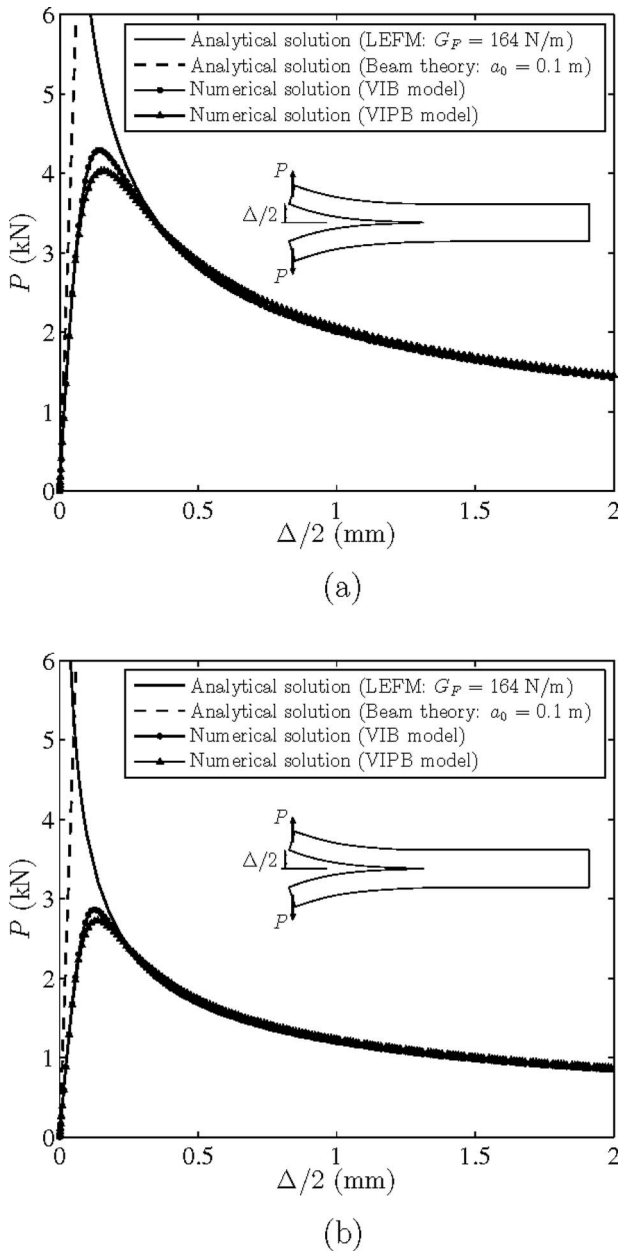

Fig. 8. Numerical simulation results of the DCB test using the VIB and the VIPB models with the localization zone size of (a) h_L=0.5 mm; (b) h_L=0.25 mm

peak load of the VIPB model is lower than that of the VIB model because of the different softening behavior as discussed previously (Fig. 6).

Validation

In order to validate the VIPB model for quasi-brittle materials, numerical simulation results are compared with previous experimental results from three-point bending (TPB) tests of plain concrete (Roesler et al. 2007a) and FRC (Roesler et al. 2007b). For the plain concrete experiments, three sizes (D=63, 150, 250 mm) of notched beam were designed with a constant thickness (t=80 mm), notch to depth ratio (a_0/D=1/3), and span to depth ratio (S/D=4) (see Fig. 9). For the FRC experiments, the beam depth was 150 mm with the thickness of 80 mm, notch to depth ratio of 1/3, and span to depth ratio of 4.

Three-Point Bending Tests of Plain Concrete

Experimental elastic and fracture parameters of concrete are presented in Table 2. The tensile strength of 4.15 MPa was measured by the splitting test (Brazilian test). The total fracture energy was obtained by the work-of-fracture method (Hillerborg 1985), and the initial fracture energy was estimated by the two-parameter fracture model (TPFM) (Jenq and Shah 1985). Finally, the strength ratio (β=0.34) in the pair-bond potential was calculated by using the critical crack tip opening displacement ($CTOD_c$) obtained from the TPFM (Park 2005).

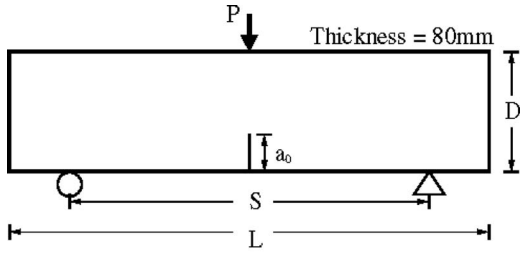

[mm]

Size (D)	Length (L)	Span (S)	Notch (a_0)
63	250	350	21
150	600	700	50
250	1000	1100	83

Fig. 9. Specimen geometry of TPB tests

Based on the concrete properties in Table 2, the constants in the modified Morse potential are evaluated by expression (23) in conjunction with the numerical simulation of the pure tension test at a localization zone size of 0.5 mm. Table 3 illustrates the calculated constants in the bond density potential for the VIB (single-bond) model, and Table 4 provides those for the VIPB (pair-bond) model. The exponents in the bond density potential are calibrated by simulating the pure tension test so that the numerical fracture parameters correspond to the material fracture parameters. In the VIPB model, the constants $(\alpha_1, m_1, \mathcal{D}_1)$ in the steep short-range potential (Ψ_1) are the same for all specimen sizes, as the potential represents the size independent initial fracture energy (G_f). However, in the shallow long-range potential (Ψ_2), the constants $(\alpha_2, m_2, \mathcal{D}_2)$ are different with respect to size,

Table 2. Elastic and Fracture Parameters of Concrete Beam Experiments by Roesler et al. (2007a)

Specimen size (mm)	Elastic modulus (GPa)	Tensile strength (MPa)	Initial fracture energy (N/m)	Strength ratio at kink point (β)	Total fracture energy (N/m)
63					119
150	32	4.15	56.6	0.34	164
250					167

Table 3. Material Properties and the Constants in the Bond Density Potential for Each Size of Beam in the VIB (Single-Bond) Model with the Localization Zone Size of 0.5 mm

Size D (mm)	E (GPa)	f_t' (MPa)	G_F (N/m)	α	m	$\mathcal{D}$ (N m/m^3)
63			119	34	315	41,960
150	32	4.15	164	23	480	60,170
250			167	22	510	61,900

Table 4. The Constants in Each Bond Density Potential for the VIPB (Pair-Bond) Model with the Localization Zone Size of 0.5 mm

	$(1-\beta)E$, $(1-\beta)f_t'$, G_f			βE, $\beta f_t'$, $G_F - G_f$		
Size D (mm)	α_1	m_1	$\mathcal{D}_1$ (N m/m^3)	α_2	m_2	$\mathcal{D}_2$ (N m/m^3)
63				19	630	25,450
150	50	215	18,760	9	1,260	50,900
250				8	1,480	54,660

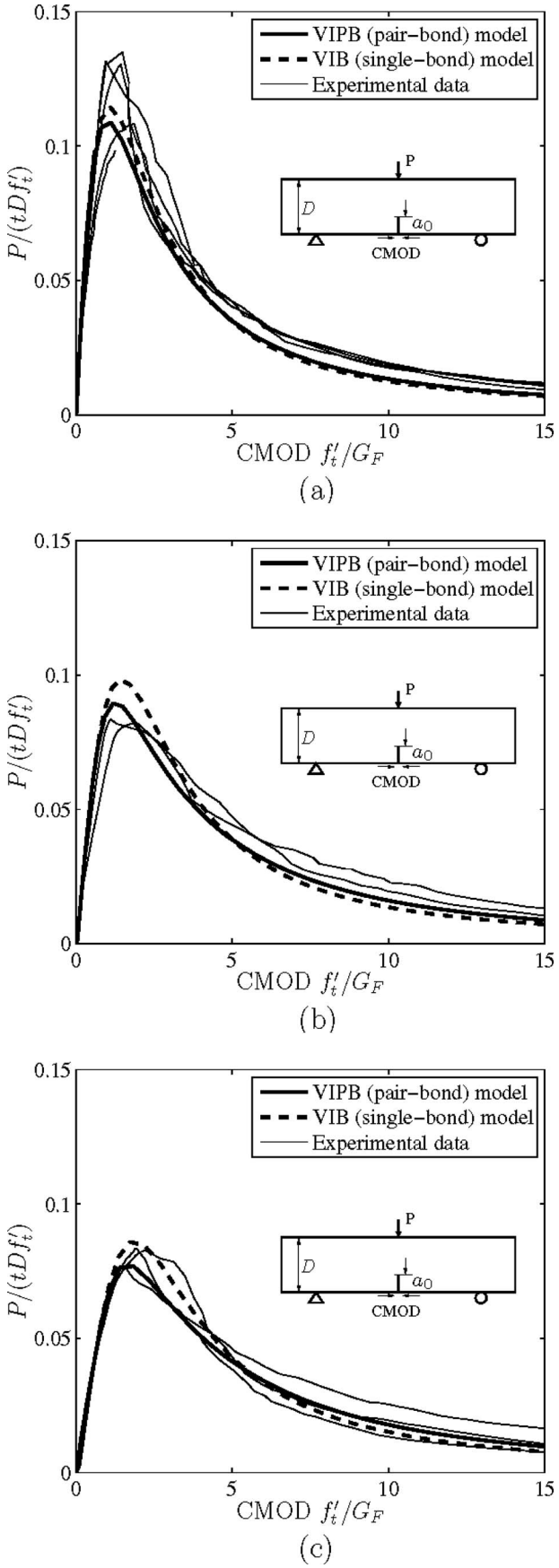

Fig. 10. Comparison of load-CMOD curves with experimental results: (a) specimen size $D=63$ mm; (b) specimen size $D=150$ mm; and (c) specimen size $D=250$ mm

J. Eng. Mech., 2008, 134(10): 856-866

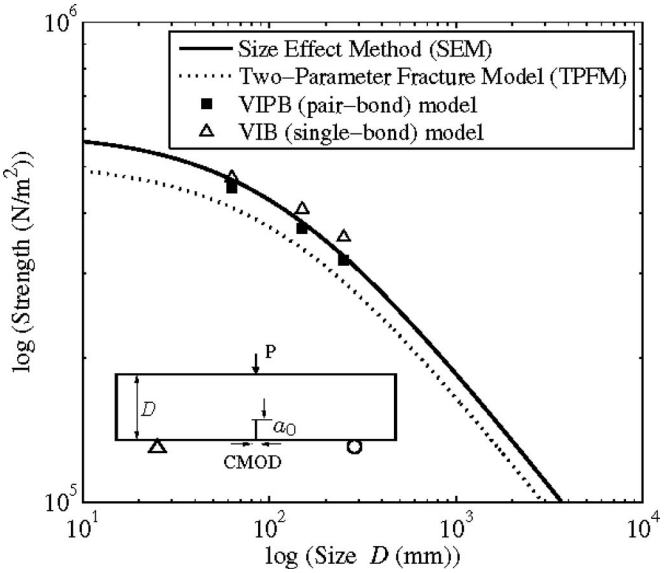

Fig. 11. Size effect for TPB fracture test configuration

due to the size dependence of the total fracture energy (G_F), as shown in Table 4. The exponent m_2 of the long-range potential is not only greater than the exponent m_1 of the short-range potential, but the exponent m_2 also increases with size. The increased specimen size produces a larger total fracture energy for a fixed cohesive strength, resulting in a shallow long-range potential. This feature corresponds well to the characteristics of the Morse potential; the larger value of m, the longer the range, and the shallower the potential (Milstein 1973).

Figs. 10(a–c) illustrate the correspondence between the numerical predictions of the VIPB model and the experimental results for each specimen size with respect to the normalized load versus crack mouth opening displacement (CMOD) curves. The VIB model slightly overestimates the peak load, due to the VIB model consisting of a single-bond potential related to the total fracture energy, whereas the VIPB model employs two different potentials, i.e., the steep short-range and the shallow long-range potential, associated with the initial fracture energy and the total fracture energy.

On Size Effect

In general, the size effect due to the scaling of geometrically similar structures can be characterized by the nominal strength of the structure, the maximum deflection, and the maximum strain (Bazant 1999). In this study, the size effect is examined by plotting the structural size (D) versus the nominal strength (σ_{Nu}), which is calculated as the peak load divided by the beam size (D) and thickness (t), as shown in Fig. 11. The solid and dashed lines are calculated, respectively, by the size effect method (SEM) (Bazant and Planas 1998) and the TPFM (Jenq and Shah 1985) through the size effect expression (Bazant and Kazemi 1990)

Table 5. Elastic and Fracture Parameters of Plain Concrete (Roesler et al. 2007b)

Elastic modulus (GPa)	Tensile strength (MPa)	Total fracture energy (N/m)	Strength ratio at kink point (β)
26.9	3.4	120	0.28

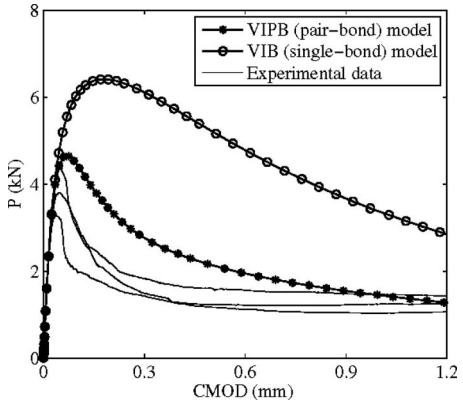

Fig. 12. Prediction of load-CMOD curves of FRC beam tests compared with experimental data

$$\sigma_{Nu} = \frac{Bf_t'}{\sqrt{1 + D/D_0}} \tag{27}$$

where the nondimensional constant, B, and the length dimensional constant, D_0, are determined by the three-point bending tests in Table 2. The numerical prediction of the VIPB model trends with the size effect expression (27), and is bounded by the SEM and the TPFM curves, as shown in Fig. 11. The single potential (VIP) model demonstrates overestimation of the strength with respect to the increase in structural size (D) for this specific example. Moreover, the strength differences between the VIB model and the VIPB model grow with respect to the increase of specimen size.

TPB Test of Fiber-Reinforced Concrete

FRC beams were cast with ordinary plain concrete and fiber volume fraction of 0.78%. Elastic and fracture parameters of the ordinary plain concrete are provided in Table 5. The total fracture energies of plain concrete and FRC are 120 and 3,531 N/m, respectively, which are obtained by the work-of-fracture method (Hillerborg 1985). Based on these experimental elastic and fracture parameters, load versus CMOD curves of the FRC beams are predicted by simulating the VIPB model and the VIB model. The simulation results are compared with the experimental data, as shown in Fig. 12. The VIPB model demonstrates a similar load-CMOD curve to experimental data, whereas the VIB model overestimates the peak load and postpeak behavior in this example.

Conclusions

A VIPB model is proposed to consider two fracture energies, the initial fracture energy (G_f) and the total fracture energy (G_F), which are essential fracture parameters to represent the fracture behavior and size effect of quasi-brittle materials, such as concrete. The initial fracture energy is related to the steep short-range bond density potential, whereas the difference between the initial fracture energy and the total fracture energy is associated with the shallow long-range bond density potential. Further, the VIPB model is extended to simulate fracture behavior of FRC in conjunction with two fracture energies, the total fracture energy of plain concrete (G_F) and the total fracture energy of FRC (G_{FRC}).

A modified Morse function (atomistic potential) is proposed for the bond density potential in the VIPB model so that the

potential function is independent of the discrete lattice parameter (l_0). The elastic modulus, cohesive strength, and fracture energy, which can be obtained by means of macroscopic experiments, determine the three constants in each modified Morse function ($m_i, \alpha_i, \mathcal{D}_i$).

The model parameters in the bond density potential are estimated from the experimental fracture parameters and a pure tension simulation. The DCB simulations are conducted simply to verify the relationship between the fracture energy (G_F) and the localization zone size (h_L). The VIPB model is validated by predicting the load-CMOD curves of three-point bending tests for both plain concrete and FRC. The later example involving FRC clearly demonstrates the advantage of the VIPB model over the usual VIB model (cf. Fig. 12).

Further, the present conceptual framework, i.e., the superposition of the two potentials, can be extended to account for other physical behaviors. For instance, the VIPB model can be changed to a virtual internal multiple-bond potential model, which can represent other interactions between fractured surfaces, e.g., friction.

Acknowledgments

The writers would like to acknowledge support from the National Science Foundation (NSF) through Grant CMMI 0800805. The writers also acknowledge support from the Center of Excellence for Airport Technology (CEAT), funded by the Federal Aviation Administration (FAA) under Research Grant Number 95-C-001 and the Univ. of Illinois. The writers appreciate the useful comments of Dr. David R. Brill to this work. The information presented in this paper is the sole opinion of the writers and does not necessarily reflect the views of the sponsors.

Notation

The following symbols are used in this paper:

- $\mathbf{C}$ or C_{IJKL} = material tangent modulus;
- $\mathcal{D}_\Omega$ = bond density function;
- $\mathcal{D}_0$ = constant bond density function;
- $\mathcal{D}_1, \mathcal{D}_2$ = bond densities for the pair-bond potential;
- E = elastic modulus;
- $\mathbf{E}$ or E_{IJ} = Lagrangian strain;
- $\mathbf{F}$ or F_{IJ} = deformation gradient;
- f_t' = tensile strength;
- G_F = (total) fracture energy;
- G_{F0} = reference fracture energy;
- G_f = initial fracture energy;
- h_L = localization zone;
- h_{L0} = reference localization zone;
- l = deformed virtual bond length;
- l_0 = undeformed virtual bond length;
- m_i = exponents in the modified Morse potential ($i=1,2$);
- $\mathbf{N}$ or N_I = outward normal to the contour;
- $\mathbf{P}$ or P_{IJ} = first Piola–Kirchhoff stress;
- $\mathbf{S}$ or S_{IJ} = second Piola–Kirchhoff stress;
- $U(l)$ = bonding potential;
- U_0 = strain energy density;
- w_f = final crack opening width;
- w_k = crack opening width at the kink point;
- w_1 = horizontal axis intercept of the initial descending line;
- $\mathbf{X}$ or X_I = Lagrangian coordinates;
- $\mathbf{x}$ or x_i = Eulerian coordinates;
- α_i = exponents in the modified Morse potential ($i=1,2$);
- β = strength ratio of the pair-bond potential;
- Γ = contour in the undeformed configuration surrounding a crack tip;
- λ, μ = Lame parameters;
- λ_2 = stretch along the X_2 direction;
- ν = Poisson's ratio;
- $\boldsymbol{\xi}$ or ξ_I = bond direction;
- σ = Cauchy stress;
- Φ = strain energy function;
- $\Psi(l)$ = bond density potential; and
- Ω = domain.

References

Anderson, T. L. (1995) *Fracture mechanics: Fundamentals and applications*, CRC, Boca Raton, Fla.

Barenblatt, G. I. (1959). "The formation of equilibrium cracks during brittle fracture: General ideas and hypotheses, axially symmetric cracks." *J. Appl. Math. Mech.*, 23(3), 622–636.

Bazant, Z. P. (1999). "Size effect on structural strength: A review." *Arch. Appl. Mech.*, 69(9–10), 703–725.

Bazant, Z. P. (2000). "Size effect." *Int. J. Solids Struct.*, 37(1–2), 69–80.

Bazant, Z. P., and Becq-Giraudon, E. (2002). "Statistical prediction of fracture parameters of concrete and implications for choice of testing standard." *Cem. Concr. Res.*, 32(4), 529–556.

Bazant, Z. P., and Kazemi, M. T. (1990). "Determination of fracture energy, process zone length and brittleness number from size effect, with application to rock and concrete." *Int. J. Fract.*, 44(2), 111–131.

Bazant, Z. P., and Planas, J. (1998). *Fracture and size effect in concrete and other quasi-brittle materials*, CRC, Boca Raton.

Belytschko, T., Liu, W. K., and Moran, B. (2000). *Nonlinear finite elements for continua and structures*, Wiley, New York.

Born, M. (1940). "On the stability of crystal lattices. I." *Proc. Cambridge Philos. Soc.*, 36, 160–172.

Dugdale, D. S. (1960). "Yielding of steel sheets containing slits." *J. Mech. Phys. Solids*, 8(2), 100–104.

Gao, H., and Ji, B. (2003). "Modeling fracture in nanomaterials via a virtual internal bond method." *Eng. Fract. Mech.*, 70(14), 1777–1791.

Gao, H., and Klein, P. (1998). "Numerical simulation of crack growth in an isotropic solid with randomized internal cohesive bonds." *J. Mech. Phys. Solids*, 46(2), 187–218.

Girifalco, L. A., and Weizer, V. G. (1959). "Application of the Morse potential function to cubic metals." *Phys. Rev.*, 114(3), 687–690.

Hillerborg, A. (1985). "The theoretical basis of a method to determine the fracture energy G_F of concrete." *Mater. Struct.*, 18(4), 291–296.

Hillerborg, A., Modeer, M., and Petersson, P. E. (1976). "Analysis of crack formation and crack growth in concrete by means of fracture mechanics and finite elements." *Cem. Concr. Res.*, 6(6), 773–781.

Jenq, Y. S., and Shah, S. P. (1985). "Two parameter fracture model for concrete." *J. Eng. Mech.*, 111(10), 1227–1241.

Klein, P., and Gao, H. (1998). "Crack nucleation and growth as strain localization on a virtual-bond continuum." *Eng. Fract. Mech.*, 61(1), 21–48.

Klein, P. A., Foulk, J. W., Chen, E. P., Wimmer, S. A., and Gao, H. (2001). "Physics-based modeling of brittle fracture: Cohesive formulations and the application of meshfree methods." *Theor. Appl. Fract. Mech.*, 37(1–3), 99–166.

Milstein, F. (1973). "Applicability of exponentially attractive and repul-

sive interatomic potential functions in the description of cubic crystals." *J. Appl. Phys.*, 44(9), 3825–3832.
Morse, P. M. (1929). "Diatomic molecules according to the wave mechanics. II: Vibrational levels." *Phys. Rev.*, 34(1), 57–64.
Nguyen, T. D., Govindjee, S., Klein, P. A., and Gao, H. (2004). "A rate-dependent cohesive continuum model for the study of crack dynamics." *Comput. Methods Appl. Mech. Eng.*, 193(30–32), 3239–3265.
Pandolfi, A., and Ortiz, M. (2002). "An efficient adaptive procedure for three-dimensional fragmentation simulations." *Eng. Comput.*, 18(2), 148–159.
Park, K. (2005). "Concrete fracture mechanics and size effect using a specialized cohesive zone model." Master's thesis, Univ. of Illinois at Urbana-Champaign, Urbana, Ill.
Park, K., Paulino, G. H., and Roesler, J. R. (2008). "Determination of the kink point in the bilinear softening model for concrete." *Eng. Fract. Mech.*, 75(13), 3806–3818.
Paulino, G. H., Song, S. H., and Buttlar, W. G. (2004). "Cohesive zone modeling of fracture in asphalt concrete." *Proc., 5th RILEM Int. Conf. on Cracking in Pavements: Mitigation, Risk Assessment and Prevention*.
Rice, J. R. (1968). "A path independent integral and the approximate analysis of strain concentration by notches and cracks." *ASME J. Appl. Mech.*, 35(2), 379–386.
Roesler, J. R., Paulino, G. H., Gaedicke, C., Bordelon, A., and Park, K. (2007b). "Fracture behavior of functionally graded concrete materials (FGCM) for rigid pavements." *Transportation Research Record. 2037*, Transportation Research Board, Washington, D.C., 40–49.
Roesler, J. R., Paulino, G. H., Park, K., and Gaedicke, C. (2007a). "Concrete fracture prediction using bilinear softening." *Cem. Concr. Compos.*, 29(4), 300–312.
Rose, J. H., Ferrante, J., and Smith, J. R. (1981). "Universal binding energy curves for metals and bimetallic interfaces." *Phys. Rev. Lett.*, 47(9), 675–678.
Shah, S. P., Swartz, S. E., and Ouyang, C. (1995). *Fracture mechanics of concrete*, Wiley, New York.
Song, S. H., Paulino, G. H., and Buttlar, W. G. (2006a). "A bilinear cohesive zone model tailored for fracture of asphalt concrete considering viscoelastic bulk material." *Eng. Fract. Mech.*, 73(18), 2829–2848.
Song, S. H., Paulino, G. H., and Buttlar, W. G. (2006b). "Simulation of crack propagation in asphalt concrete using a cohesive zone model." *J. Eng. Mech.*, 132(11), 1215–1223.
Tadmor, E. B., Ortiz, M., and Phillips, R. (1996). "Quasicontinuum analysis of defects in solids." *Philos. Mag. A*, 73(6), 1529–1563.
Thiagarajan, G., Hsia, K. J., and Huang, Y. (2004). "Finite-element implementation of virtual internal bond model for simulating crack behavior." *Eng. Fract. Mech.*, 71(3), 401–423.
Van Mier, J. G. M. (1996) *Fracture processes of concrete: Assessment of material parameters for fracture models*, CRC, Boca Raton, Fla.
Xu, X. P., and Needleman, A. (1994). "Numerical simulation of fast crack growth in brittle solids." *J. Mech. Phys. Solids*, 42(9), 1397–1434.
Zhang, P., Klein, P., Huang, Y., Gao, H., and Wu, P. D. (2002). "Numerical simulation of cohesive fracture by the virtual-internal-bond model." *CMES—Comput. Model. Eng. Sci.*, 3(2), 263–277.
Zhang, Z., and Paulino, G. H. (2005). "Cohesive zone modeling of dynamic failure in homogeneous and functionally graded materials." *Int. J. Plast.*, 21(6), 1195–1254.
Zhang, Z., Paulino, G. H., and Celes, W. (2007). "Extrinsic cohesive modeling of dynamic fracture and microbranching instability in brittle materials." *Int. J. Numer. Methods Eng.*, 72(8), 893–923.